Publication V

Anssi Sinervo and Antero Arkkio. Modeling two-pole cage induction machine equipped with embedded force actuator. In *Tenth International Conference on Vibrations in Rotating Machinery (VIRM10)*, Woodhead Publishing, London, September 2012.

Modeling two-pole cage induction machine equipped with embedded force actuator

A Sinervo, A Arkkio
Aalto University School of Electrical Engineering, Finland

ABSTRACT

This paper is about modeling of a two-pole cage induction machine equipped with a embedded force actuator for active control of lateral rotor vibrations. A fourth-order complex-valued linear differential-equation is derived to describe how the control voltage affects the rotor vibration. The model is identified using complex exponent sweeps since the model has explicit time-dependence. Validation measurements are done with white-noise signals. Time-domain fit with the presented techniques is better than with traditional ones.

1 INTRODUCTION

Rotor vibration is a problem in electrical machines. The vibration causes bearings to wear and can lead to a catastrophic mechanical failure if the rotor hits the stator of the machine while running. This can happen if the rotor has a mass unbalance and the machine is running at a natural resonance frequency of the rotor. Traditionally, this is prevented in designing by making sure the natural frequencies are above or below the operational speed range of the machine. Avoiding the critical frequencies sets constrains on optimizing the performance and efficiency of the machine.

Some of the vibration problems can be solved with magnetic bearings. However, the magnetic bearings will not help if the rotor is too long and the vibration is caused by rotor bending. The magnetic bearings only support the rotor from the ends. Chiba [1] presented an idea of building the magnetic bearing into an induction machine. If a two-pole induction machine is fitted with a four-pole addition stator winding, the four-pole winding can be used as an embedded force actuator [2]. This allows the rotor to be supported from the middle.

The embedded force actuator produces force as the four-pole magnetic field interacts with the two-pole field. The sum of these fields is non-symmetric around the rotor. The magnetic pull is proportional to the square of the magnetic flux density. If the flux is denser at one side of the rotor than the other side, there will be a total magnetic pull. The non-symmetric magnetic flux can be created with the two windings but it also arises as a result of rotor eccentricity [3].

It has already been shown [4] that the embedded force actuator can be used to control rotor vibrations in a two-pole induction machine but the control algorithms require a model of the machine [5]. The models in [4] were identified for one operation point only and required an identification measurement at that operation point to fully remove the vibrations. The operation point here means the values of the supply frequency, two-pole flux density, and slip. The control model, the force produced by the actuator voltage, depends strongly on the operation point. It would be very convenient to parameterize the dependence.

In this paper, the control model has been derived. The parametric model is not presented but the paper presents measurement techniques that can be useful when seeking the parametric model. The model will have a explicit time-dependence due to the stator and rotor slots [6][7] preventing the use of traditional methods. The proposed control model could be used with the control method presented in [8].

2 MACHINE TO BE MODELED

The machine to be modeled is a two-pole induction machine with an additional four-pole winding in the stator. The two-pole winding is controlled separately to maintain the wanted rotation speed or torque and the four-pole winding is used to keep the rotor centred. It is assumed that the four-pole magnetic flux does not affect the two-pole magnetic flux. This assumption is valid if the two-pole flux is much stronger than the four-pole flux. It is further assumed that the two-pole flux density amplitude and frequency, and the rotor rotation frequency are constant and given as parameters.

Measurements were conducted with a 30 kW test machine. The rotor of the test machine had a long shaft on external bearings. The rotor vibrations were measured from the shaft with four eddy-current sensors. The sensors measured displacement in horizontal and vertical directions at both ends of the machine, figure 1. The rotor displacement was calculated as an average of both ends. The shaft was slightly (<50 μm) bowed and twisted, thus the force actuator was attempting to prevent further bending of the rotor instead of trying to centre the both sides perfectly. The air-gap length was 1 mm.

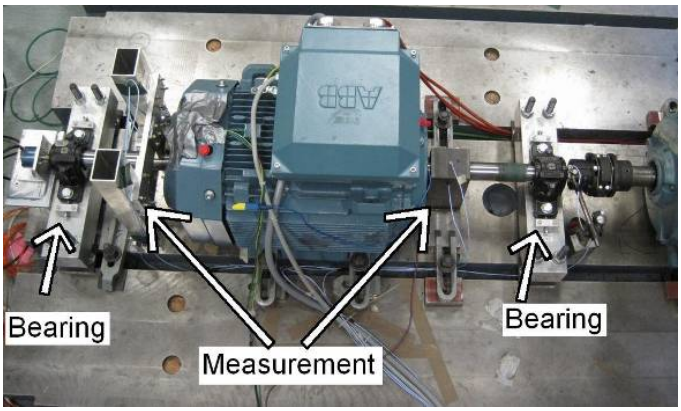

Figure 1. Test rig. The shaft is supported by external bearings. The rotor displacement is measured at the shaft at both ends of the machine in horizontal and in vertical directions.

The actuator, the four-pole winding, was voltage controlled. The control voltage was supplied with amplifiers via a discrete-to-analog port and the control signal was calculated on a computer. Each of the three phases had its own amplifier and the star-point was grounded. The control code had the constraint that the sum of voltage must be zero, thus there were only two-degrees of freedom.

The two-pole winding was supplied with a synchronous generator that allowed the frequency and amplitude of the voltage to be set independently. The two-pole flux was measured with a two-phase search-coil. The rotation speed of the machine was measured with a tachometer. A same size induction machine was used to control the slip. The load machine was connected to the shaft via a flexible coupling, seen

at right in figure 1, that prevented the propagation of radial forces from one machine to the other. Details of the windings were presented in [6].

3 DERIVING THE MODEL

Radial movement of the rotor core can be modeled with a second-order linear differential equation. The mechanical system is assumed to be symmetric with respect to the horizontal and vertical directions. Thus, the mass of the rotor *m*, the mechanical damping *d*, and the spring constant of the rotor shaft *k* are all real valued scalar constants. The displacement of the rotor core $\underline{z}$ has been presented as a complex variable. The real and imaginary parts denote horizontal and vertical displacement, respectively.

$$\left(m\frac{\mathrm{d}^2}{\mathrm{d}t^2} + d\frac{\mathrm{d}}{\mathrm{d}t} + k \right)\underline{z} = \underline{F}_{\mathrm{m}} + \underline{F}_{\mathrm{e,2}} + \underline{F}_{\mathrm{e,h}} \tag{1}$$

The radial force in (1) has been divided into three parts: the mechanical force from mass unbalance $\underline{F}_{\mathrm{m}}$, the magnetic force from the interaction of the two- and four-pole magnetic fluxes $\underline{F}_{\mathrm{e,2}}$, and the magnetic force from the other spatial harmonics of the magnetic flux density in the air-gap $\underline{F}_{\mathrm{e,h}}$. The mechanical force rotates at the rotation speed ω_{r} and it has constant amplitude if the rotation speed does not change. The force is proportional to the rotor mass and the square of the rotation speed.

The magnetic force from the interaction of the two- and four-pole magnetic flux density in the air-gap is the one that is used for the active control. It was derived in [6] that this force can be written as (2) where C_{F} is a constant containing physical dimensions of the rotor, $\hat{B}_1$ is the two-pole flux density amplitude and $\underline{\hat{B}}_2^k$ the four-pole flux density space-vector. The four-pole flux has to be presented in rotating coordinates to obtain force in stator frame of reference. Superscript k denotes a frame of reference that rotates with half the rotation speed of the two-pole flux $\omega_1/2$.

$$\underline{F}_{\mathrm{e,2}} = C_{\mathrm{F}}\hat{B}_1\underline{\hat{B}}_2^k \tag{2}$$

The third part of the force in (1) comprises the magnetic forces due to the slotting and the interaction of the unipolar and the two-pole flux density components. It acts as a negative spring constant but has also an explicitly time-varying part [7].

$$\underline{F}_{\mathrm{e,h}} = c_{\mathrm{h1}}\hat{B}_1^{\,2}\underline{z} + \underline{c}_{\mathrm{h2}}\hat{B}_1^{\,2}\underline{z}^{*}e^{\mathrm{j}2\omega_1 t} \tag{3}$$

The superscript star denotes complex conjugate, ω_1 is the angular rotation speed of the two-pole flux which is the same as the two-pole supply frequency. It will be later shown that the second term on right side of (3) will cause vibration frequencies to pair up. For example, static eccentricity will cause a force at double supply-frequency. The second term is caused by the non-rotating magnetic fields, with respect to the stator, with pole-pair numbers equal to the multiples of the number of stator slots, including zero [6].

In (3), it is assumed that there are no currents induced by the higher harmonics causing dynamics. The four-pole flux does induce currents in the rotor cage and the four-pole actuator winding. The currents change the flux that would be caused by the rotor eccentricity, as indicated by (4).

$$\underline{\hat{B}}_2^{\mathrm{k}} = \frac{\underline{z}}{2\delta_{\mathrm{e}}}\hat{B}_1 e^{\mathrm{j}(\omega_1 - 2\omega_{\mathrm{k}})t} + \frac{\mu_0}{\delta_{\mathrm{e}}}k_{\mathrm{r}}\underline{\hat{i}}_{r,2}^{\mathrm{k}} + \frac{\mu_0 N_2 k_{\mathrm{c}}}{\delta_{\mathrm{e}}}\underline{\hat{i}}_{\mathrm{s},2}^{\mathrm{k}} \tag{4}$$

The four-pole flux, and thus the eccentricity, is linked back to the currents via the voltage equations (5) and (6).

$$\underline{\hat{u}}_{\mathrm{c}}^{\mathrm{k}} = R_{\mathrm{c}}\underline{\hat{i}}_{\mathrm{s},2}^{\mathrm{k}} + \mathrm{j}\omega_1 L_{\mathrm{c},\sigma}\underline{\hat{i}}_{\mathrm{s},2}^{\mathrm{k}} + L_{\mathrm{c},\sigma}\frac{\mathrm{d}}{\mathrm{d}t}\underline{\hat{i}}_{\mathrm{s},2}^{\mathrm{k}} + \mathrm{j}\omega_1 A_2 N_2 \underline{\hat{B}}_2^{k} + \frac{\mathrm{d}}{\mathrm{d}t}A_2 N_2 \underline{\hat{B}}_2^{k} \tag{5}$$

$$0 = R_{\mathrm{r}}\underline{\hat{i}}_{r,2}^{\mathrm{k}} + \mathrm{j}(\omega_1 - 2\omega_{\mathrm{r}})L_{\mathrm{r},\sigma}\underline{\hat{i}}_{r,2}^{\mathrm{k}} + L_{\mathrm{r},\sigma}\frac{\mathrm{d}}{\mathrm{d}t}\underline{\hat{i}}_{\mathrm{r},2}^{\mathrm{k}} + \mathrm{j}(\omega_1 - 2\omega_{\mathrm{r}})\underline{\hat{B}}_2^{k} + \frac{\mathrm{d}}{\mathrm{d}t}\underline{\hat{B}}_2^{k} \tag{6}$$

The force can be controlled via the actuator voltage $\underline{\hat{u}}_{\mathrm{c}}^{\mathrm{k}}$ which has been presented as a space-vector that defines the three phase voltages. The voltage equations must be written in the same rotating coordinates, denoted by k, as the four-pole flux. This shows by ω_1 appearing in the equations. The constants in equations (4)–(6) are not important at this time, see [6] for reference.

The voltage equations (5) and (6) can be combined into one second-order differential equation that combined with the force and flux equations, (2) and (4) respectively, gives the force $\underline{F}_{\mathrm{e},2}$.

$$\left(\frac{\mathrm{d}^2}{\mathrm{d}t^2} + \underline{a}'_2\frac{\mathrm{d}}{\mathrm{d}t} + \underline{a}'_3\right)\underline{F}_{\mathrm{e},2} = \left(b'_1\frac{\mathrm{d}}{\mathrm{d}t} + \underline{b}'_2\right)\underline{\hat{u}}_{\mathrm{c}}^{\mathrm{k}} + \left(c'_1\frac{\mathrm{d}^2}{\mathrm{d}t^2} + \underline{c}'_2\frac{\mathrm{d}}{\mathrm{d}t} + \underline{c}'_3\right)\underline{z} \tag{7}$$

The force depends on the control voltage and the rotor displacement. When the magnetic force due to slot harmonics and unipolar flux (3) is substituted into the mechanical equation (1), it becomes

$$\left(m\frac{\mathrm{d}^2}{\mathrm{d}t^2} + d\frac{\mathrm{d}}{\mathrm{d}t} + k - c_{\mathrm{h}1}\hat{B}_1^{\,2}\right)\underline{z} = \underline{F}_{\mathrm{m}} + \underline{F}_{\mathrm{e},2} + \underline{c}_{\mathrm{h}2}\hat{B}_1^{\,2}\underline{z}^{*}\mathrm{e}^{\mathrm{j}2\omega_1 t} \tag{8}$$

This will result in a pair of second-order differential equations for the rotor displacement. The equation pair has two inputs, the control voltage and the mechanical unbalance force.

Though there is explicit time dependence in (8), the model is linear and the mechanical unbalance force can be removed using superposition. The two equations (7) and (8) combine into

$$\left(\frac{\mathrm{d}^4}{\mathrm{d}t^4} + \underline{a}_3\frac{\mathrm{d}^3}{\mathrm{d}t^3} + \underline{a}_2\frac{\mathrm{d}^2}{\mathrm{d}t^2} + \underline{a}_1\frac{\mathrm{d}}{\mathrm{d}t} + \underline{a}_0\right)\underline{z}' = \left(\underline{b}_1\frac{\mathrm{d}}{\mathrm{d}t} + \underline{b}_0\right)\underline{\hat{u}}_{\mathrm{c}}^{\mathrm{k}} + \left(\underline{h}_2\frac{\mathrm{d}^2}{\mathrm{d}t^2} + \underline{h}_1\frac{\mathrm{d}}{\mathrm{d}t} + \underline{h}_0\right)\underline{z}'^{*}\mathrm{e}^{\mathrm{j}2\omega_1 t} \tag{9}$$

which will be the control model. The model gives the dynamic rotor displacement response $\underline{z}'$ to the control voltage $\underline{\hat{u}}_{\mathrm{c}}^{\mathrm{k}}$. All the coefficients are complex valued and the explicit time-dependence means that standard techniques for time-invariant systems cannot be used to identify them.

4 FREQUENCY RESPONSE

Equation (9) is a special case of equation (10).

$$\left(a_n\left(\frac{\mathrm{d}}{\mathrm{d}t}\right)^n + a_{n-1}\left(\frac{\mathrm{d}}{\mathrm{d}t}\right)^{n-1} + \cdots + a_1\left(\frac{\mathrm{d}}{\mathrm{d}t}\right) + a_0\right)\underline{z}' = \left(b_m\left(\frac{\mathrm{d}}{\mathrm{d}t}\right)^m + b_{m-1}\left(\frac{\mathrm{d}}{\mathrm{d}t}\right)^{m-1} + \cdots \right.$$

$$\left. \cdots + b_1\left(\frac{\mathrm{d}}{\mathrm{d}t}\right) + b_0\right)\underline{\hat{u}}_{\mathrm{c}}^{\mathrm{k}} + \left(h_l\left(\frac{\mathrm{d}}{\mathrm{d}t}\right)^l + h_{l-1}\left(\frac{\mathrm{d}}{\mathrm{d}t}\right)^{l-1} + \cdots + h_1\left(\frac{\mathrm{d}}{\mathrm{d}t}\right) + h_0\right)\underline{z}'^{*}\mathrm{e}^{\mathrm{j}\omega t} \quad (10)$$

If the control voltage is written as a Fourier-series, (11), the exact solution to (10) will be (12).

$$\underline{\hat{u}}_{\mathrm{c}}^{\mathrm{k}} = \sum_{k=-\infty}^{\infty} \underline{u}_k \mathrm{e}^{\mathrm{j}\omega_k t} \quad (11)$$

$$\underline{z}' = \sum_{k=-\infty}^{\infty} \left\{\underline{A}_k \mathrm{e}^{\mathrm{j}\omega_k t} + \underline{B}_k{}^{*}\mathrm{e}^{\mathrm{j}(\omega-\omega_k)t}\right\} \quad (12)$$

The superscript star on $\underline{B}_k$ denotes complex conjugate. For every input frequency ω_k there are two output frequencies, ω_k and $2\omega_1 - \omega_k$ since $\omega = 2\omega_1$ in the special case.

If we define characteristic polynomials for (10) as

$$\underline{P}_a(x) \doteq \underline{a}_n\left(x\right)^n + \underline{a}_{n-1}\left(x\right)^{n-1} + \cdots + \underline{a}_1\left(x\right) + \underline{a}_0 \quad (13)$$

$$\underline{P}_b(x) \doteq \underline{b}_m\left(x\right)^m + \underline{b}_{m-1}\left(x\right)^{m-1} + \cdots + \underline{b}_1\left(x\right) + \underline{b}_0 \quad (14)$$

$$\underline{P}_h(x) \doteq \underline{h}_l\left(x\right)^l + \underline{h}_{l-1}\left(x\right)^{l-1} + \cdots + \underline{h}_1\left(x\right) + \underline{h}_0 \quad (15)$$

the Fourier coefficients of the solution will be

$$\underline{A}_k = \frac{\underline{P}_a{}^{*}(\mathrm{j}\omega - \mathrm{j}\omega_k)\underline{P}_b(\mathrm{j}\omega_k)}{\underline{P}_a(\mathrm{j}\omega_k)\underline{P}_a{}^{*}(\mathrm{j}\omega - \mathrm{j}\omega_k) - \underline{P}_h(\mathrm{j}\omega_k)\underline{P}_h{}^{*}(\mathrm{j}\omega - \mathrm{j}\omega_k)}\underline{u}_k \quad (16)$$

$$\underline{B}_k = \frac{\underline{P}_h{}^{*}(\mathrm{j}\omega - \mathrm{j}\omega_k)\underline{P}_b(\mathrm{j}\omega_k)}{\underline{P}_a{}^{*}(\mathrm{j}\omega - \mathrm{j}\omega_k)\underline{P}_a(\mathrm{j}\omega_k) - \underline{P}_h(\mathrm{j}\omega_k)\underline{P}_h{}^{*}(\mathrm{j}\omega - \mathrm{j}\omega_k)}\underline{u}_k \quad (17)$$

This can be shown by substituting (11)–(17) into (10).

The Fourier coefficient of the control voltage $\underline{u}_k$ and the Fourier coefficients of the displacement response $\underline{A}_k$ and $\underline{B}_k$ in (16) and (17) can be measured and then used to find the parameters of (9). Theoretically $\underline{u}_k$ is obtained from a simple integral.

$$\frac{1}{T}\int_0^T \underline{\hat{u}}_{\mathrm{c}}^{\mathrm{k}}\mathrm{e}^{-\mathrm{j}\omega_k t}\mathrm{d}t = \frac{1}{T}\int_0^T \sum_{i=-\infty}^{\infty}\left\{\underline{u}_i \mathrm{e}^{\mathrm{j}(\omega_i-\omega_k)t}\right\}\mathrm{d}t = \underline{u}_k \quad (18)$$

In practice, the measurements are done with some sampling frequency and the discrete Fourier transformation can be used.

$$\underline{u}_k \approx \frac{1}{N}\sum_{n=1}^{N} \underline{\hat{u}}_{\mathrm{c}}^{\mathrm{k}}(n\Delta t)\mathrm{e}^{-\mathrm{j}\omega_k n\Delta t} \quad (19)$$

The same integral for the displacement response gives the coefficient $\underline{A}_k$, corresponding to the control voltage component $\underline{u}_k$, plus complex conjugate of coefficient $\underline{B}_{p-k}$ that corresponds to the control voltage component $\underline{u}_{p-k}$.

$$\frac{1}{T}\int_0^T \underline{z}' \mathrm{e}^{-\mathrm{j}\omega_k t}\mathrm{d}t = \frac{1}{T}\int_0^T \sum_{i=-\infty}^{\infty} \left\{ \underline{A}_i \mathrm{e}^{\mathrm{j}(\omega_i-\omega_k)t} + \underline{B}_i^{\,*} \mathrm{e}^{\mathrm{j}(\omega-\omega_i-\omega_k)t} \right\} \mathrm{d}t = \underline{A}_k + \underline{B}_{p-k}^{\,*} \tag{20}$$

The control voltage component $\underline{u}_{p-k}$ means input voltage at frequency $\omega-\omega_k$ or, in the special case (9), $2\omega_1-\omega_k$. The classic frequency response of the control voltage to the rotor displacement can be seen as a sum of the two overlapping responses.

If the input signal for the identification is band-limited in such way that it does not have frequencies $2\omega_1-\omega_k$, the integral (20) gives only $\underline{A}_k$. The other coefficient in (17), $\underline{B}_k$ would then be given by integral

$$\frac{1}{T}\int_0^T \left(\underline{z}'^{*} \mathrm{e}^{\mathrm{j}\omega t}\right) \mathrm{e}^{-\mathrm{j}\omega_k t}\mathrm{d}t = \frac{1}{T}\int_0^T \sum_{i=-\infty}^{\infty} \left\{ \underline{A}_i^{\,*} \mathrm{e}^{\mathrm{j}(\omega-\omega_i-\omega_k)t} + \underline{B}_i \mathrm{e}^{\mathrm{j}(\omega_i-\omega_k)t} \right\} \mathrm{d}t = \underline{B}_k + \underline{A}_{p-k}^{\,*} \tag{21}$$

One way to create such a band-limited signal is to use sine sweeps or in the case of complex variables, complex exponent sweeps.

5 MEASUREMENT TECHNIQUES

The measurements were done using complex exponent sweeps. The modeled range was limited between -100 Hz to 100 Hz, since it was known that all the important Eigen values of the system would be within this range. It would have been enough if the frequencies were measured in two parts, to and from the two-pole supply frequency which was 25 Hz during the measurements. Instead, the measurements were done in eight parts that each covered a 25 Hz span.

Figure 2 shows the input voltage spectrum of one of the measurements and the rotor displacement response to the input voltage. There were clearly two separate frequency bands in the response corresponding to $\underline{A}_k$ and $\underline{B}_k$ of (12). The $\underline{B}_k$ band appears mirrored due to the complex conjugate. The left half of the input band is responsible for the right half of the respond band. Two respond bands were collected from each measurement and then combined to form two complete responses.

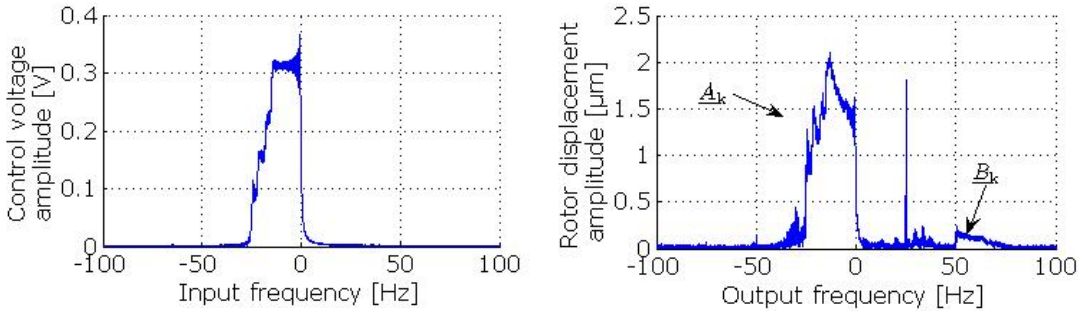

Figure 2. Control voltage and rotor displacement response. One control-voltage frequency-band awakes two separate frequency bands in the output.

Before calculating the frequency responses, the rotor displacement caused by the mechanical unbalance force $\underline{F}_{\mathrm{m}}$ had to be calculated and subtracted from the

measured total displacement. This displacement was considered as a deterministic disturbance. Because the system is assumed to be linear, the disturbance can be measured by having the control voltage zero.

The disturbance will be a function of the rotor angle as is $\underline{F}_{\mathrm{m}}$ but it will also be a function of the two-pole field angle, $\omega_1 t$, because of the last term in (8). Thus, it will be a function of the two angles and can be represented as a periodic surface. It was difficult to replicate exactly the same phase for the field angle and the rotation angle as in the control-voltage-off measurement because of the limited sampling frequency. Therefore, the surface was discretized in a matrix form after which the disturbance was interpolated from the matrix using the measured rotation and two-pole field angles. Figure 3 shows the measured displacement, the calculated disturbance, and the resulting response for one of the measurements.

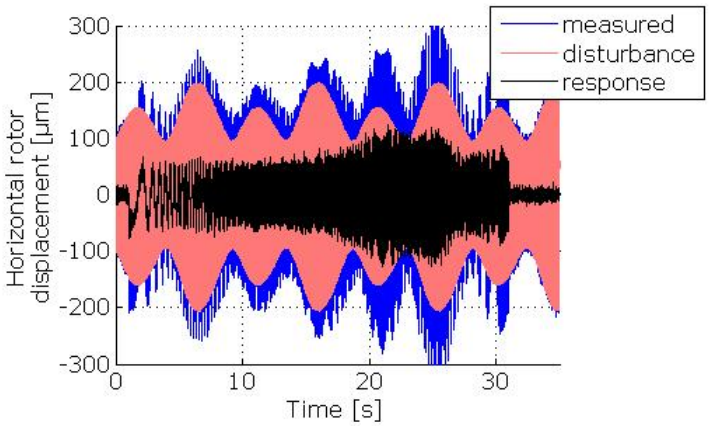

Figure 3. Horizontal rotor displacement response to complex exponent sweep from 0 to 25 Hz.

6 RESULTS

The parameters of the model (9) were optimized to match the measurements in the frequency domain using cost function

$$\mathrm{Cost} = \sum_k \left(\left| \tilde{\underline{A}}_k - \hat{\underline{A}}_k \right| + \left| \tilde{\underline{B}}_k - \hat{B}_k \right| \right) \tag{22}$$

where $\hat{\underline{A}}_k$ and $\hat{B}_k$ are calculated from (16) and (17), respectively, and $\tilde{\underline{A}}_k$ and $\tilde{\underline{B}}_k$ from (20) and (21), respectively. The two-pole supply frequency was 25 Hz, two-pole flux density 0.5 T, and slip 0.42 %. Figure 4 shows the results, $\underline{A}_k / \underline{u}_k$ on the left and $\underline{B}_k / \underline{u}_k$ on the right. The fit was excellent at least for $\underline{A}_k$. Error in phase is less than 10 degrees everywhere.

The phase response indicates the difference between the direction of the force and the direction of the control voltage vector. The zero direction for the control voltage was defined based on the physical orientation of the four-pole winding. The physical orientations of the windings were known with respect to the rotor displacement measurement. At the defined zero direction and at zero frequency, the flux density vector of the four-pole winding would point towards the positive horizontal axis of the frame of reference of the displacement measurement.

The x-axis in figure 4 is the control voltage frequency in the rotating coordinates k. The real frequency of the phase voltages is the input frequency plus the two-pole

supply frequency 25 Hz. The vibration frequency of $\underline{A}_k$ part, left in the figure, will be the same as input frequency but for $\hat{B}_k$ the output frequency is twice the two-pole supply frequency minus the input frequency as can be seen from (12). If $\hat{B}_k$ is presented as a function of the output frequency, figure 4 right side curves would be mirrored around +25 Hz. For example the +82 Hz spike corresponds to whirling motion at -32 Hz. A negative frequency means the rotor centre whirls against the rotation of the rotor.

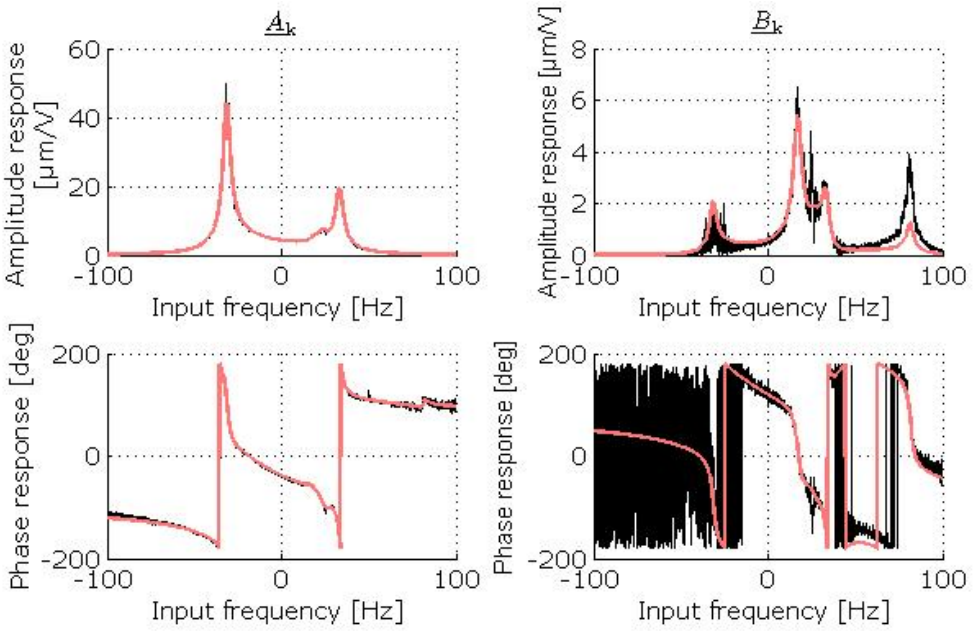

Figure 4. The measured and modelled frequency response. The left side is $\underline{A}_k$ and the right side is $\underline{B}_k$.

To validate the results and to calculate the fit, a band-limited (<200 Hz) signal was supplied to both the real and imaginary parts of the control voltage. The disturbance was measured with the control voltage zero and removed from the measured rotor displacement. The model (9) was simulated using the same input voltage as in the measurement. The fit was calculated as the Euclidean norm of the error between the measured, x, and the simulated, $\hat{x}$, rotor displacements divided by the deviation of the measured rotor displacement, (23). In (23), $|x|$ is the average of the measured horizontal rotor displacement. The validation result in the vertical direction has been presented in figure 5.

$$\text{Fit} = 1 - \frac{1}{2}\frac{\|x - \hat{x}\|}{\|x - |x|\|} - \frac{1}{2}\frac{\|y - \hat{y}\|}{\|y - |y|\|} \tag{23}$$

The fit between the measured and simulated rotor displacement was 84.5 % with the validation data. If the explicitly time-depending part was left out, i.e. $\underline{h}_i$ terms in (9) set to zero, the fit dropped to 75 %. A second set of data measured the same way as the validation data was used to identify a time-invariant model for comparison. Using MATLAB® system identification function 'pem' (calculates prediction error estimate), the best fit achieved was 82 % even when the order of the model was increased.

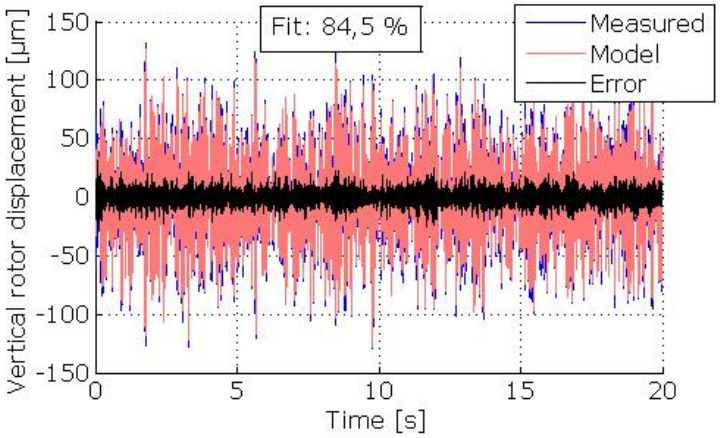

Figure 5. Fit to validation data measured using band-limited white-noise input.

7 CONCLUSIONS

A simple linear but periodically time-varying model was derived for the rotor vibration control of a two-pole induction machine with an extra four-pole stator winding. The model had only four Eigen values, two from mechanical and two from electrical origin. The frequency response of the system was theoretically derived and shown to be a sum of two overlapping time-invariant frequency responses. It was shown that the two parts can be measured separately using band-limited input-signals.

The measurement technique using complex exponent sweeps gave a clear frequency response with low noise level. The model seemed to fit the measurements and could be used for model based control. There was some error at input frequencies around +82 Hz that could be caused by some unmodeled dynamics of the slot harmonics of the air-gap magnetic field or the unipolar flux.

The validation of the model was done by supplying a random signal as the control voltage. The same signal was to simulate the model. The time-domain fit with the model was better than with the tested time-invariant techniques. The improvement was not much but the main benefit of the model is that it should capture the real physics of the machine and should therefore be easier to parameterize.

Acknowledgment

The research project was funded by the Academy of Finland. The authors are also grateful to a Finnish national doctoral programme The Graduate School in Electrical Energy Engineering (GSEEE) for financial support, and Walter Ahlström foundation, Finnish Foundation for Technology Promotion, KAUTE foundation, The Association of Electrical Engineers in Finland, and Ulla Tuominen foundation for financial encouragement.

References

[1] Chiba, A., Power, D., and Rahman, M., "Characteristics of a bearingless induction motor," *IEEE Transactions on Magnetics,* , vol. 27, no. 6, pp. 5199 –5201, Nov. 1991.

[2] Chiba, A., Fukao, T., Ichikawa, O., Oshima, M., Takemoto, M., and Dorrell, D. G., *Magnetic Bearings and Bearingless Drives*. Burlington, MA: Elsevier Newnes Press, 2005.

[3] Smith, A. and Dorrell, D., "Calculation and measurement of unbalanced magnetic pull in cage induction motors with eccentric rotors. part i: Analytical model," *Proc. IEE Electric Power Applications*, vol. 143(3), pp. 193–201, 1996.

[4] Laiho, A., Sinervo, A., Tammi, K., Arkkio, A., and Zenger, K., "Attenuation of harmonic rotor vibration in a cage rotor induction machine by a self-bearing force actuator," *IEEE Transactions on Magnetics*, vol. 45, no. 12, pp. 5388–5398, December 2009.

[5] Orivuori, J., Zenger, K., Sinervo, A., and Laiho, A., "Active control of rotor vibration in an electric machine by cascaded optimal and convergent control methods," *International Journal of Acoustics and Vibration*, 2012.

[6] Sinervo, A., Laiho, A., and Arkkio, A., "Low-frequency oscillation in rotor vibration of a two-pole induction machine with extra four-pole stator winding," *Magnetics, IEEE Transactions on*, vol. 47, no. 9, pp. 2292 –2302, sept. 2011.

[7] Laiho, A., Tammi, K., and Vidquist, V., "Modelling of flexural rotor vibration and time-periodic system dynamics in a two-pole cage induction machine equipped with a self-bearing force actuator," in *in Proceedings of the IFACWorkshop on Periodic Systems*, Turkey, 2010.

[8] Sinervo, A. and Arkkio, A., "Controlling rotor vibrations of two-pole induction machine under loaded operation," in *19th International Congress on Sound and Vibration (ICSV19)*, Vilnius, Lithuania, July 2012.